Electronic Supplementary Information

Reaction of OH radicals with CH_3NH_2 in the gas phase: Experimental (11.7-177.5 K) and computed rate coefficients (10-1000 K)

Daniel González,[a] Anxo Lema-Saavedra,[b] Sara Espinosa,[a] Emilio Martínez-Núñez,[c] Antonio Fernández-Ramos,[bc] André Canosa,[d] Bernabé Ballesteros[ae], and Elena Jiménez*[ae]

[a.] *Departamento de Química Física, Facultad de Ciencias y Tecnologías Químicas. Universidad de Castilla-La Mancha. Avda. Camilo José Cela 1B, 13071, Ciudad Real, Spain.*
[b.] *Centro Singular de Investigación en Química Biológica y Materiales Moleculares (CIQUS), Campus Vida, Universidade de Santiago de Compostela, C/Jenaro de la Fuente s/n, 15782, Santiago de Compostela, Spain.*
[c.] *Departamento de Química Física, Facultade de Química, Campus Vida, Universidade de Santiago de Compostela, Avda. das Ciencias s/n, 15782, Santiago de Compostela, Spain.*
[d.] *CNRS, IPR (Institut de Physique de Rennes)-UMR 6251. Université de Rennes, F-35000 Rennes, France*
[e.] *Instituto de Investigación en Combustión y Contaminación Atmosférica (ICCA). Universidad de Castilla-La Mancha. Camino de Moledores s/n, 13071, Ciudad Real, Spain.*

Experimental conditions

Table S1 shows a summary of all the experimental conditions employed for the kinetic study of the OH+CH_3NH_2 reaction.

Table S1 Experimental conditions employed in this work as a function of the temperature and density of the buffer gas.

T / K	% He	% Ar	% N_2	n / 10^{16} cm^{-3}	F_{buffer} / slpm	$F_{CH3NH2/buffer}$ / sccm	F_{H2O2} / sccm	F_{total} / slpm	f_{CH3NH2} / 10^{-3}
11.7 ± 0.7	100			6.88 ± 0.62	4.76 – 5.47	8.5 – 90.3	100.3 – 163.4	4.93 – 5.57	21
29.2 ± 1.1	90		10	8.68 ± 0.53	2.97 – 3.03	6.6 – 58.0	83.4	3.06 – 3.14	21 – 30
36.2 ± 1.2	100			17.7 ± 0.9	12.41 – 12.82	8.2 – 93.9	79.0 – 102.2	12.57 – 12.93	27
45.3 ± 1.3	20		80	4.23 ± 0.28	1.29 – 1.39	11.1 – 54.9	33.9 – 70.4	1.39 – 1.46	11 – 23
50.5 ± 1.6			100	1.50 ± 0.12	1.13 – 1.27	28.5 – 161.9	26.5	1.29 – 1.31	25
49.9 ± 1.8			100	3.67 ± 0.32	1.26 – 1.38	11.2 – 67.6	54.5	1.38 – 1.44	17
49.9 ± 1.4	74		26	8.33 ± 0.41	3.82 – 3.96	8.2 – 101.3	42.4 – 51.6	3.95 – 4.01	27
52.1 ± 0.5		100		19.5 ± 0.3	4.50 – 4.92	47.5 – 411.7	25.6	4.92 – 5.02	1 – 2
64.2 ± 1.7 [a]			100	2.23 ± 0.15	3.77 – 3.96	23.1 – 201.5	20.2	3.99 – 4.00	49 – 71
64.1 ± 1.6	20		80	4.63 ± 0.27	1.67 – 1.85	26.4 – 138.7	15.4	1.86 – 1.87	8
64.4 ± 0.6		70	30	17.4 ± 0.3	4.63 – 4.95	26.0 – 84.6	20.9	4.86 – 4.97	7
77.4 ± 1.0			100	2.38 ± 0.08	0.64 – 0.70	11.1 – 62.6	17.1	0.72 – 0.73	28
76.0 ± 0.8		40	60	15.0 ± 0.3	4.53 – 4.89	62.1 – 400.2	26.4	4.95 – 4.98	2
89.5 ± 0.6			100	18.2 ± 0.3	7.06 – 7.31	20.0 – 104.9	54.5	7.18 – 7.40	10
89.1 ± 0.7		100		43.3 ± 0.5	6.98 – 7.28	47.4 – 197.4	25.6	7.17 – 7.36	2 – 5
107.0 ± 0.5			100	4.90 ± 0.06	1.07 – 1.17	11.2 – 95.5	3.9 – 11.3	1.17 – 1.18	15
106.0 ± 0.6		100		14.0 ± 0.1	1.37 – 1.68	47.5 – 325.7	6.9	1.70 – 1.73	2
135.0 ± 0.8			100	29.4 ± 0.5	5.82 – 6.11	53.4 – 325.7	35.8	6.15 – 6.20	10
158.8 ± 0.6			100	7.40 ± 0.07	0.78 – 1.06	10.2 – 231.5	4.4 – 9.1	1.00 – 1.07	16 – 47
177.5 ± 1.2			100	6.71 ± 0.11	0.39 – 0.65	40.8 – 292.0	2.9 – 7.7	0.60 – 0.70	11

[a]Continuous flow conditions. slpm, standard litres per minute; sccm, standard cubic centimetres per minute.

Verification of the CH_3NH_2 dilution factor in the storage bulb *via* UV spectroscopy

In order to check the value of $f_{CH_3NH_2}$ and to be confident in the calculated [CH_3NH_2] in the jet, UV spectroscopy (λ=189-260 nm) was used to measure the amount of CH_3NH_2 in the storage bulbs. The UV experimental system used in this work was previously described.[1,2] It consists in a deuterium light source (StellarNet, model: SL4 DT-200) which was used to irradiate the gas sample contained in a absorption cell (pathlength, l =107.15 cm). After light dispersion in a concave grating (StellarNet, model: Black-Comet BLK-C) the transmitted light was detected in a charge-coupled device (CCD). The spectral resolution was 3 nm.

Firstly, the UV absorption cross sections (σλ) between 190 and 260 nm were determined by recording five UV spectra at different total pressures of pure CH_3NH_2 in the UV cell ($P_{UV\ cell}$ = 0.29-0.66 mbar), as shown in Figure S1.A. The accomplishment of the Beer-Lambert's law, i.e. a linear relationship between the absorbance (in base e) A_λ and [CH_3NH_2] was checked for some selected wavelengths. The σλ values at these selected wavelengths were extracted from the slope of plots presented in Figure S1.B. After checking that these individual σλ are in agreement with those from the literature[3], the cross section evolution in the wavelength range 190-260 nm was obtained by averaging σλ derived from the five UV spectra from Figure S1.A by simply rearranging the Beer-Lambert's law equation.

$$\sigma_\lambda = \frac{A_\lambda}{l[CH_3NH_2]} \qquad \text{(EI)}$$

Figure S2 shows the UV spectrum (in terms of the absorption cross sections) of pure CH_3NH_2 along with the literature spectrum (dark line) from Hubin-Franskin *et al.*[3] Note that the fine structure of methylamine can be revealed in Hubin-Franskin *et al.*'s spectrum because of their higher spectral resolution (0.05 nm).[3] Then, a reference UV spectrum of CH_3NH_2 ($A_{\lambda,ref}$ *versus* λ – dashed line in Fig. S3.A) of a known concentration ($[CH_3NH_2]_{ref} = 8\times10^{15}$ $cm^{-3,}$ Figure S3.A) was built to be used in the quantification of CH_3NH_2 in the storage bulb. For such a quantification, the UV spectrum of several samples of the diluted CH_3NH_2 mixture ($P_{UV\ cell}$ = 13-123 mbar of diluted methylamine) was compared with the UV reference spectrum.

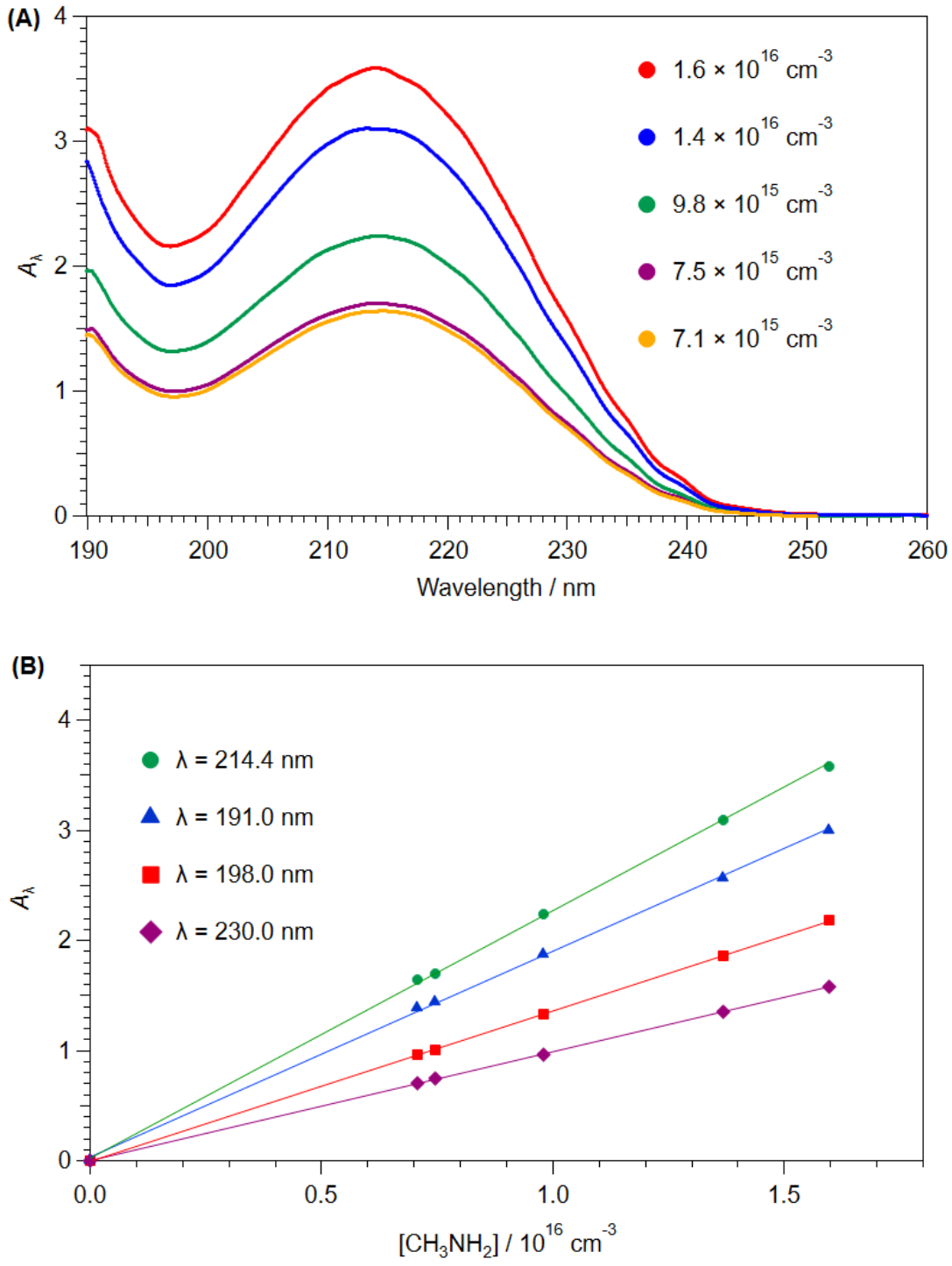

Figure S1. (A) UV spectra of the pure CH_3NH_2 at five different total pressures (or concentrations). (B) Beer-Lambert plot for some wavelengths.

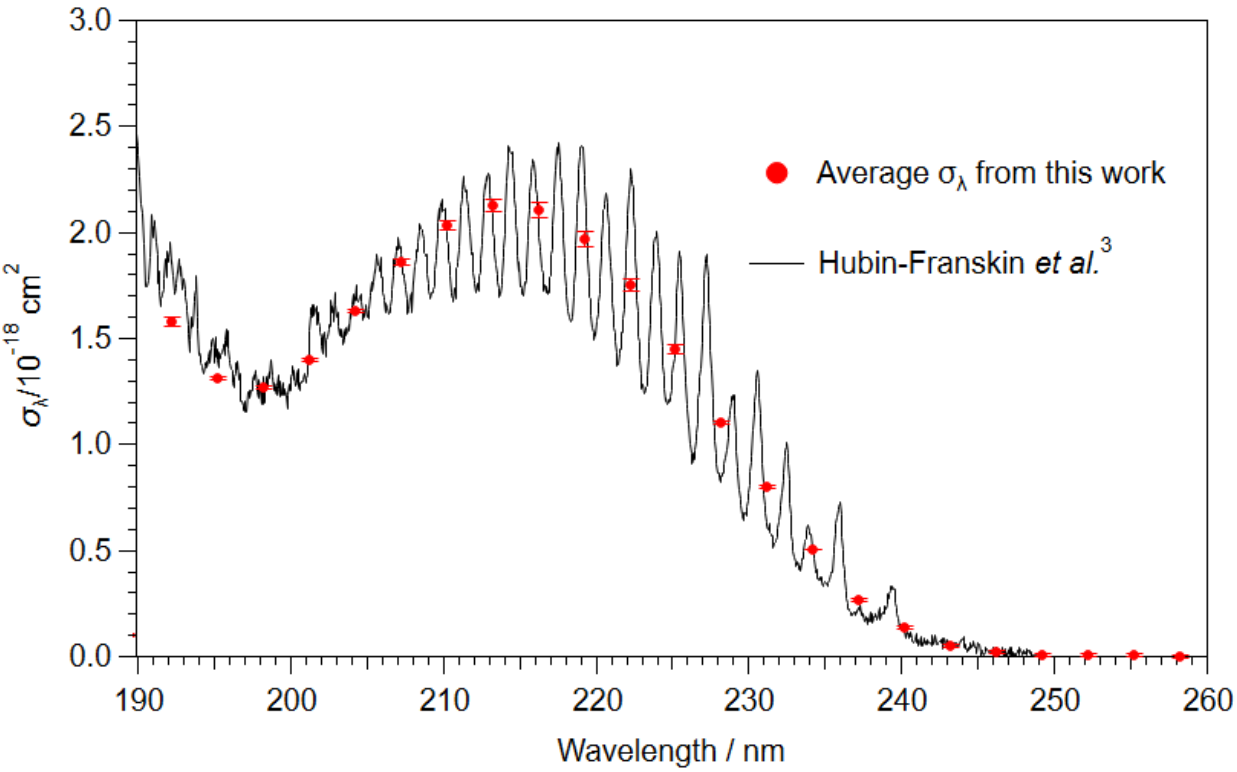

Figure S2. Comparison of the UV spectrum of CH_3NH_2 (dots), in terms of the absorption cross sections, with that from the literature (black solid line).

As the pathlength and σ_λ are constant, the methylamine concentration in the UV cell from the storage bulb, $[CH_3NH_2]_{exp}$, was obtained from the slope of $A_{\lambda,exp}$ *versus* $A_{\lambda,ref}$ plots, according to EII.

$$A_{\lambda,exp} = \frac{[CH_3NH_2]_{exp}}{[CH_3NH_2]_{ref}} A_{\lambda,ref} \qquad \text{(EII)}$$

Figure S3.B shows the excellent linearity of such a plots. The values of $f_{CH_3NH_2}$ were then derived from $[CH_3NH_2]_{exp}$ (in molecules cm^{-3}) taking into account the total pressure in the UV cell and the conversion factors.

$$[CH_3NH_2]_{exp} = f_{CH_3NH_2} \frac{P_{UV\ cell}(\text{Torr})\, N_A(\text{molecule}^{-1})}{R(\text{Torr cm}^3\ \text{molecule}^{-1}\ \text{K}^{-1})T(\text{K})} \qquad \text{(EIII)}$$

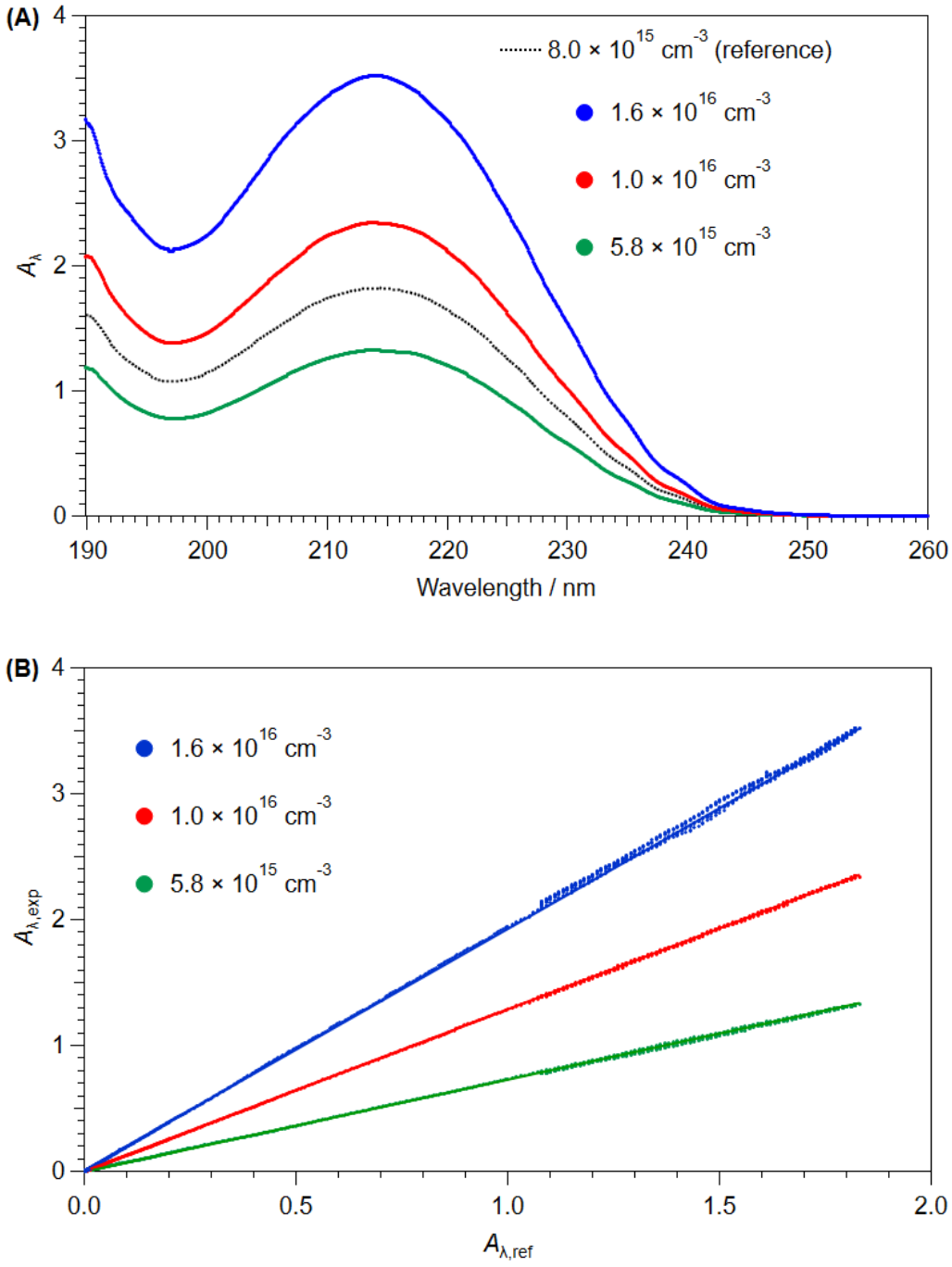

Figure S3. (A) Examples of the UV spectrum of CH_3NH_2 from the storage bulb at three different pressures (or concentrations) of methylamine with the built spectrum of reference. (B) Plot of E.I for the data presented in the upper panel.

Aerodynamic characterization of He23K-HP Laval nozzle in pulsed mode

In this work, a new operational condition in pulsed mode of the He23K-HP Laval nozzle has been aerodynamically characterized, resulting in a jet temperature of (49.9 ± 1.8) in nitrogen as shown in Table S1, and used for the kinetic measurements. This condition was previously characterized in continuous mode, yielding a jet temperature of (51.6 ± 1.7) K for such a nozzle.[4] The method to characterize the jet, based on impact pressure measurements with a Pitot tube (Kulite model XCQ-062), has been already described elsewhere.[4–11] For comparison purposes the operational conditions such as the Mach number (M), temperature (T), n_{jet}, pressure (P), hydrodynamic time (t_{hydro}), F_{total}, the pressure in the reservoir (P_{res}) and in the reaction chamber (P_{ch}) are listed in the Table S2, for both conditions in the continuous and pulsed mode as well as their spatial profile of the gas temperature and density (see Figure S4). Note that the main difference in the Table S2 is the F_{total}, where in the pulsed mode it is reduced by around 89%, making it more suitable from the economical point of view.

Table S2. Operational conditions in continuous and pulsed mode for the He23K-HP Laval nozzle.

	Continuous Mode	*Pulsed Mode*
M	4.88	5.02
T / K	51.6 ± 1.7	49.9 ± 1.8
n_{jet} /10^{16} cm^{-3}	4.17 ± 0.35	3.65 ± 0.32
P / mbar	0.30 ± 0.04	0.26 ± 0.03
t_{hydro} / µs	777	733
F_{total} / slpm[a]	13.95	1.58
P_{res} / mbar	136.24	136.59
P_{ch} / mbar	0.279	0.279

[a] Slpm, standard liter per minutes.

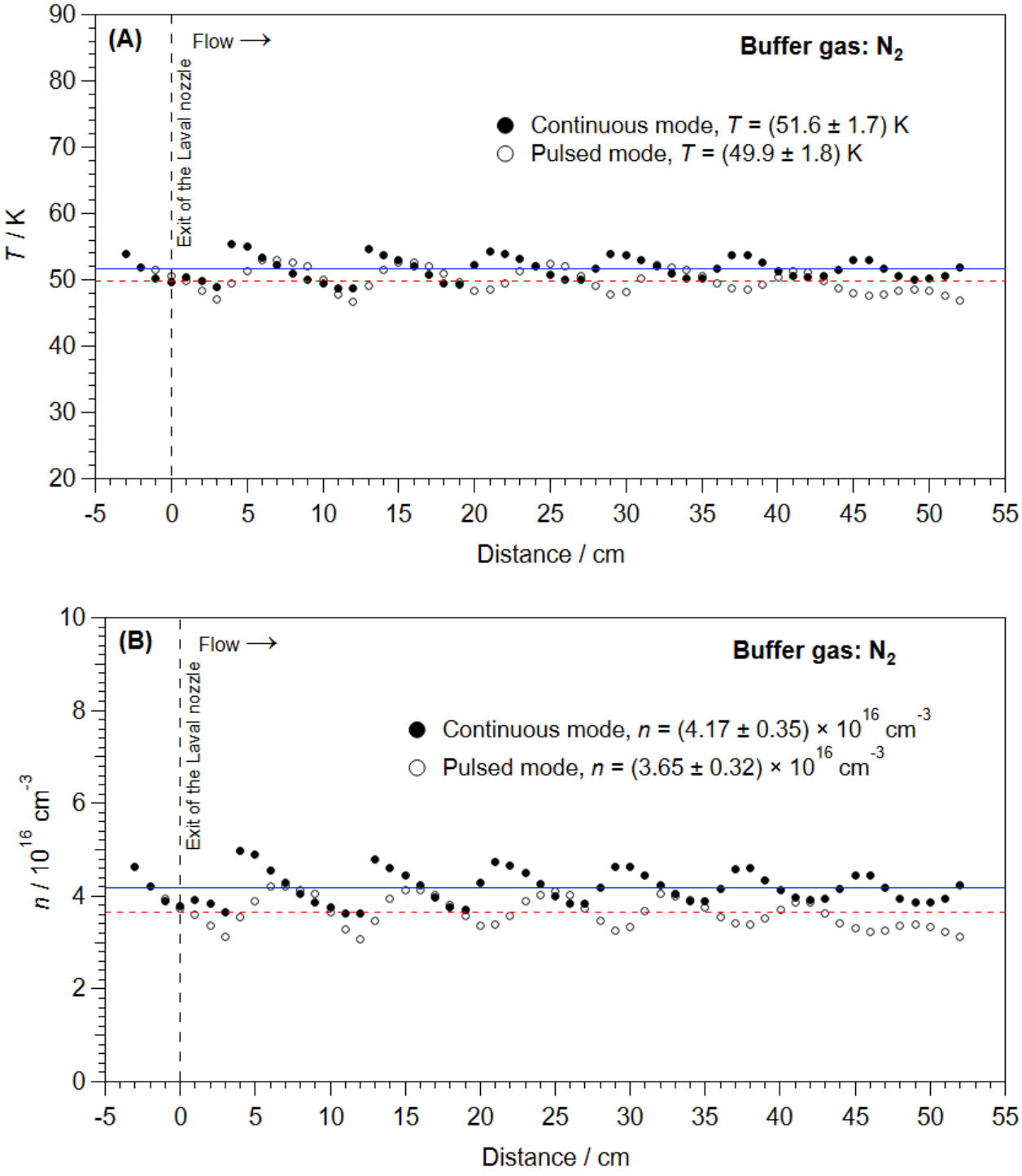

Figure S4. The spatial profile of the gas temperature (A) and gas density (B) in the uniform supersonic flow in the pulsed and continuous mode. Average gas temperature and density for the continuous condition (solid blue lines) and for the pulsed (dashed red lines) are also depicted.

Downward curvature in the bimolecular plots

We obtained k(T) at each temperature from the linear region of the k'-k'_0 vs [CH_3NH_2] plot, where the concentration of methylamine had to be kept low enough to ensure reliable values of k(T). The range of values of [CH_3NH_2] where the linearity is maintained is shown in Table 2 of the main text. Beyond these values, at higher [CH_3NH_2], a downward curvature has been observed. This observation has been usually observed in the CRESU experiments and discussed elsewhere.[1,4,6,7,9,12] It can be due to a dimerization process, in which the formation of $(CH_3NH_2)_2$ is favoured at low temperatures and high gas densities. Therefore, the amount of "free" CH_3NH_2 would be much less, leading to lower values of k(T). In Figure S5, the curvature for the lowest temperatures used in this study, 11.7 and 29.2 K, can be observed. The data represented by white squares were neglected, whereas the black squares were taken into account for the determination of k(T).

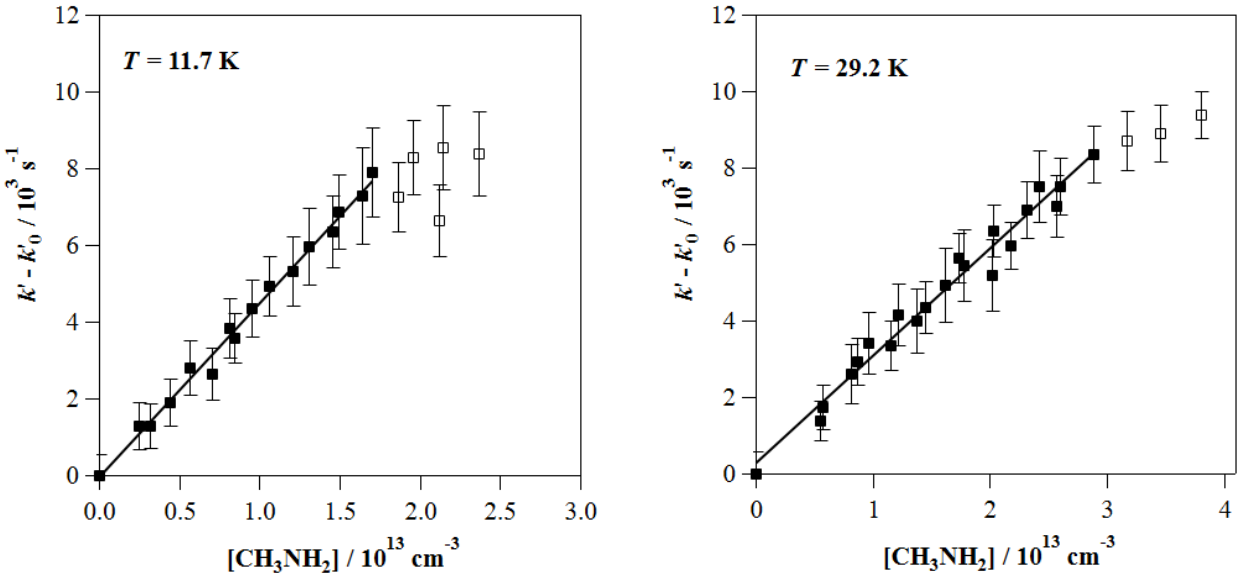

Figure S5. Examples of downward curvature in the bimolecular plots at 11.7 and 29.2 K.

References

1 S. Blázquez, D. González, E. M. Neeman, B. Ballesteros, M. Agúndez, A. Canosa, J. Albaladejo, J. Cernicharo and E. Jiménez, *Phys. Chem. Chem. Phys.*, 2020, **22**, 20562–20572.

2 E. M. Neeman, D. González, S. Blázquez, B. Ballesteros, A. Canosa, M. Antiñolo, L. Vereecken, J. Albaladejo and E. Jiménez, *J. Chem. Phys.*, 2021, **155**, 034306.

3 M.-J. Hubin-Franskin, J. Delwiche, A. Giuliani, M.-P. Ska, F. Motte-Tollet, I. C. Walker, N. J. Mason, J. M. Gingell and N. C. Jones, *J. Chem. Phys.*, 2002, **116**, 9261–9268.

4 E. Jiménez, M. Antiñolo, B. Ballesteros, A. Canosa and J. Albaladejo, *Phys. Chem. Chem. Phys.*, 2016, **18**, 2183–2191.

5 S. Blázquez, D. González, A. García-Sáez, M. Antiñolo, A. Bergeat, F. Caralp, R. Mereau, A. Canosa, B. Ballesteros, J. Albaladejo and E. Jiménez, *ACS Earth Sp. Chem.*, 2019, **3**, 1873–1883.

6 A. J. Ocaña, S. Blázquez, A. Potapov, B. Ballesteros, A. Canosa, M. Antiñolo, L. Vereecken, J. Albaladejo and E. Jiménez, *Phys. Chem. Chem. Phys.*, 2019, **21**, 6942–6957.

7 M. Antiñolo, M. Agundez, E. Jimenez, B. Ballesteros, A. Canosa, G. El Dib, J. Albaladejo and J. Cernicharo, *Astrophys. J.*, 2016, **823**, 25.

8 A. J. Ocaña, S. Blázquez, B. Ballesteros, A. Canosa, M. Antiñolo, J. Albaladejo and E. Jiménez, *Phys. Chem. Chem. Phys.*, 2018, **20**, 5865–5873.

9 A. J. Ocaña, E. Jiménez, B. Ballesteros, A. Canosa, M. Antiñolo, J. Albaladejo, M. Agúndez, J. Cernicharo, A. Zanchet, P. del Mazo, O. Roncero and A. Aguado, *Astrophys. J.*, 2017, **850**, 28.

10 E. Jiménez, B. Ballesteros, A. Canosa, T. M. Townsend, F. J. Maigler, V. Napal, B. R. Rowe and J. Albaladejo, *Rev. Sci. Instrum.*, 2015, **86**, 45108.

11 A. Canosa, A. J. Ocaña, M. Antiñolo, B. Ballesteros, E. Jiménez and J. Albaladejo, *Exp. Fluids*, 2016, **57**, 1–14.

12 I. R. Sims, J. L. Queffelec, A. Defrance, C. RebrionRowe, D. Travers, P. Bocherel, B. R. Rowe and I. R. Sims, *J. Chem. Phys.*, 1994, **100**, 4229–4241.

Electronic structure data

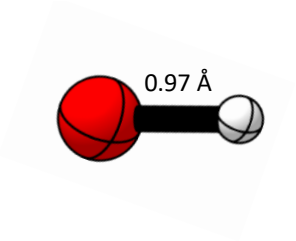

Figure S6: OH

Energies (in Hartree):
M08-HX/MG3S: -75.727155
RI-CCSD(T)-F12/cc-pVTZ-F12: -75.670360

Cartesian coordinates (in Å):

O	0.000000	0.000000	0.107793
H	0.000000	0.000000	-0.862342

Frequency (in cm^{-1}):
3796.82

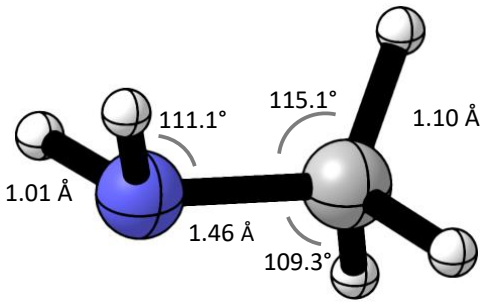

Figure S7: Methylamine

Energies (in Hartree):

M08-HX/MG3S:	-95.864308
RI-CCSD(T)-F12/cc-pVTZ-F12:	-95.737336

Cartesian coordinates (in Å):

C	0.704472	0.000000	0.017786
N	-0.746305	0.000000	-0.118910
H	1.115125	-0.878907	-0.486120
H	1.115125	0.878906	-0.486121
H	1.074864	0.000001	1.053050
H	-1.153907	0.813721	0.322424
H	-1.153906	-0.813722	0.322424

Frequencies (in cm^{-1}):

297.49	832.78	969.24	1090.48	1168.46
1339.44	1450.65	1493.63	1511.71	1664.43
3000.99	3085.81	3122.88	3556.95	3640.08

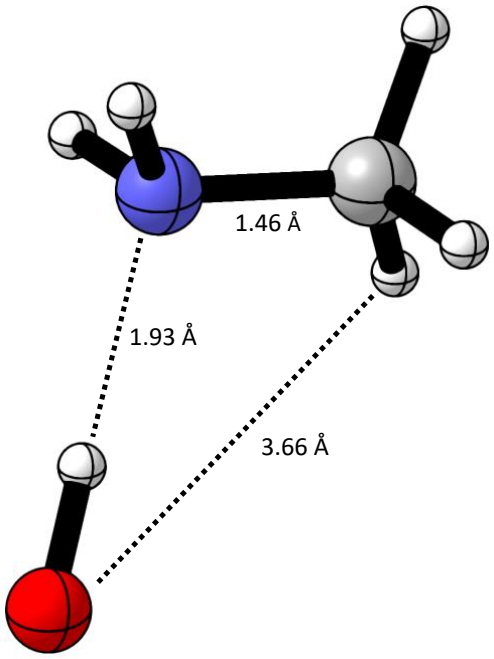

Figure S8: C1

Energies (in Hartree):

M08-HX/MG3S:	-171.605582
RI-CCSD(T)-F12/cc-pVTZ-F12:	-171.421557

Cartesian coordinates (in Å):

C	1.436608	0.515303	-0.000006
N	0.566684	-0.661895	0.000029
H	1.216804	1.125251	-0.879015
H	2.508421	0.282057	-0.001034
H	1.218341	1.124212	0.880112
H	0.744289	-1.239868	-0.812521
H	0.745238	-1.240634	0.811824
O	-2.216773	0.201227	-0.000025
H	-1.285346	-0.119390	0.000664

Frequencies (in cm^{-1}):

56.50	108.79	219.75	329.50	603.86
701.70	924.16	976.87	1080.19	1185.42
1339.01	1453.70	1495.18	1511.06	1659.01
3026.97	3105.58	3136.99	3500.97	3545.02
3623.08				

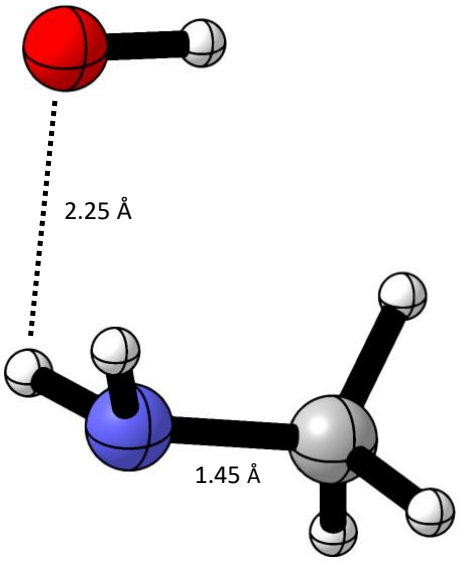

Figure S9: C2

Energies (in Hartree):

M08-HX/MG3S:	-171.597150
RI-CCSD(T)-F12/cc-pVTZ-F12:	-171.411351

Cartesian coordinates (in Å):

C	1.316773	-0.448699	-0.000000
N	0.533336	0.769368	-0.000001
H	1.964144	-0.465598	0.880377
H	0.737788	-1.387003	0.000008
H	1.964132	-0.465605	-0.880386
H	-0.035333	0.900133	-0.824703
H	-0.035326	0.900139	0.824706
O	-1.851550	-0.145558	-0.000000
H	-1.416992	-1.010984	0.000004

Frequencies (in cm^{-1}):

90.86	113.54	144.72	176.38	362.61
411.11	725.78	961.69	1101.91	1146.79
1320.32	1453.59	1494.57	1504.70	1653.49
2968.50	3083.35	3128.88	3573.12	3665.30
3814.83				

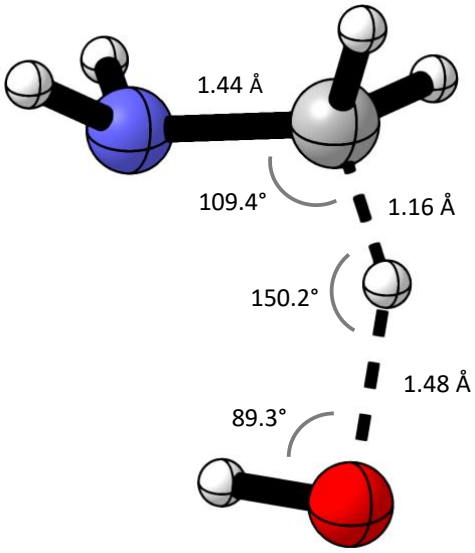

Figure S10: TS1

Energies (in Hartree):

M08-HX/MG3S:	-171.590104
RI-CCSD(T)-F12/cc-pVTZ-F12:	-171.405976

Cartesian coordinates (in Å):

C	-0.584388	0.735175	0.006022
N	-1.133790	-0.590475	-0.013289
H	0.572978	0.672140	0.059211
H	-0.876656	1.335946	0.873204
H	-0.800572	1.276038	-0.916684
H	-1.486099	-0.903400	0.877671
H	-1.825290	-0.742999	-0.730019
O	1.820884	-0.124192	0.005357
H	1.291420	-0.921911	-0.149348

Frequencies (in cm^{-1}):

-1215.70	90.32	138.43	234.53	381.81
610.79	763.98	959.51	1031.07	1121.98
1297.50	1373.44	1393.88	1465.68	1651.64
1735.22	3057.00	3145.32	3601.04	3695.39
3780.71				

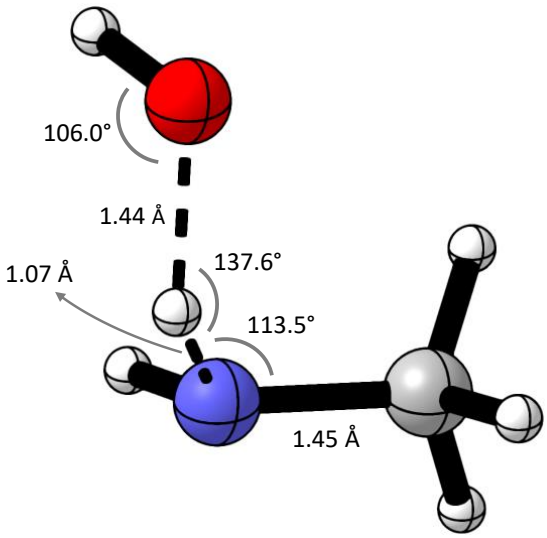

Figure S11: TS2a

Energies (in Hartree):

M08-HX/MG3S:	-171.592267
RI-CCSD(T)-F12/cc-pVTZ-F12:	-171.408612

Cartesian coordinates (in Å):

C	1.281083	-0.439106	0.043302
N	0.453163	0.732725	-0.139234
O	-1.659479	-0.279320	-0.057205
H	-0.531138	0.507851	-0.488672
H	0.414505	1.317476	0.687972
H	1.228744	-1.057308	-0.853949
H	2.320661	-0.127331	0.189758
H	0.981202	-1.053486	0.900958
H	-1.996778	0.152917	0.736401

Frequencies (in cm^{-1}):

-651.51	101.57	131.53	179.33	369.90
658.65	732.56	979.61	1091.54	1107.88
1315.70	1433.39	1470.43	1494.20	1615.60
2408.65	3024.60	3088.87	3143.81	3585.89
3847.77				

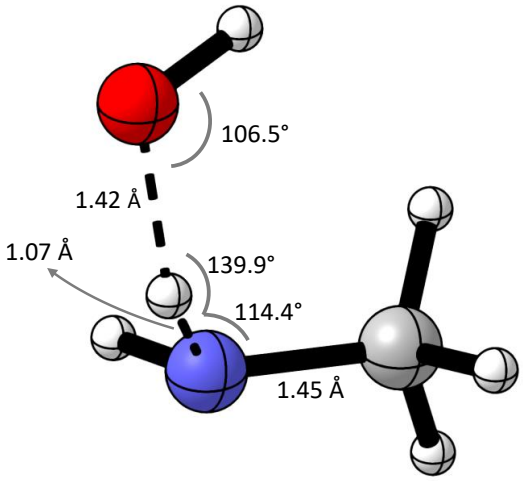

Figure S12: TS2b

Energies (in Hartree):

M08-HX/MG3S:	-171.592117
RI-CCSD(T)-F12/cc-pVTZ-F12:	-171.408533

Cartesian coordinates (in Å):

C	1.311272	-0.418029	-0.004209
N	0.434531	0.728108	-0.080619
O	-1.742381	-0.149139	-0.021637
H	-0.550844	0.508430	-0.441481
H	0.360999	1.226959	0.798717
H	1.261991	-0.975738	-0.941237
H	2.342594	-0.075361	0.133035
H	1.081992	-1.102650	0.824575
H	-1.467036	-0.977105	0.389070

Frequencies (in cm^{-1}):

-662.40	133.70	149.50	174.67	365.54
679.84	730.19	992.01	1096.63	1115.08
1323.88	1435.35	1475.38	1498.25	1575.27
2354.85	3004.71	3077.22	3136.13	3590.86
3851.36				

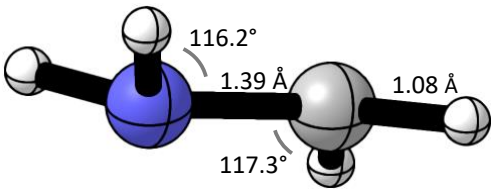

Figure S13: CH_2NH_2

Energies (in Hartree):

M08-HX/MG3S:	-95.205217
RI-CCSD(T)-F12/cc-pVTZ-F12:	-95.078591

Cartesian coordinates (in Å):

C	0.724209	0.000000	0.070780
N	-0.651916	0.000000	-0.089515
H	1.242765	-0.932015	-0.102493
H	1.242765	0.932015	-0.102493
H	-1.133685	0.834784	0.203452
H	-1.133685	-0.834784	0.203452

Frequencies (in cm^{-1}):

436.90	567.08	641.25	930.94	1251.21
1316.43	1478.89	1651.96	3180.44	3293.87
3598.92	3704.78			

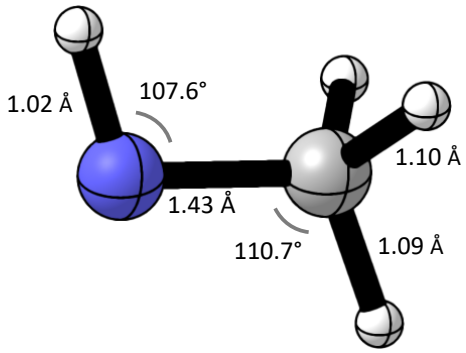

Figure S14: CH_3NH

Energies (in Hartree):

M08-HX/MG3S:	-95.190422
RI-CCSD(T)-F12/cc-pVTZ-F12:	-95.066989

Cartesian coordinates (in Å):

C	-0.626180	-0.013266	-0.000000
N	0.798707	0.152951	-0.000000
H	-0.962451	-0.583956	-0.879639
H	-0.962451	-0.583952	0.879642
H	-1.127113	0.957021	-0.000002
H	1.218147	-0.780172	0.000000

Frequencies (in cm^{-1}):

239.30	949.48	1001.85	1076.74	1329.71
1392.47	1474.57	1477.87	2979.42	3028.78
3119.91	3457.75			

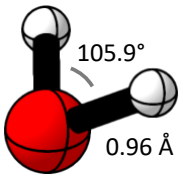

Figure S15: H_2O

Energies (in Hartree):
M08-HX/MG3S: -76.428023
RI-CCSD(T)-F12/cc-pVTZ-F12: -76.369182

Cartesian coordinates (in Å):

O	0.000000	0.000000	-0.115336
H	-0.000000	-0.763193	0.461343
H	-0.000000	0.763193	0.461343

Frequencies (in cm^{-1}):
1634.67 3898.90 3998.57

Torsional potential fitting parameters

The internal rotation of the C...O and of N...O atoms in the transition state structures was fitted to a Fourier series of the type:

$$V(x) = V_0 \sum_{i}^{n_{max}} a_i \cos(ix) + b_i \sin(ix) \tag{E.IV}$$

The paremeters of the series are listed below:

Table S3: C...O rotation

i	a_i	i	a_i
1	-324.41263	9	+0.44521
2	-91.35068	10	+0.46381
3	-35.42786	11	+0.48420
4	-4.88020	12	+1.11992
5	+6.99607	13	+0.71109
6	+9.38253	14	+0.66953
7	+5.74164	15	+0.14618
8	+2.82477	16	+0.32311

(a) $V_0 = +430.73925$ and $b_i = 0$.

Table S4: N...O rotation

i	a_i	b_i
1	-163.57383	-465.21085
2	-135.80805	+125.93875
3	-0.61629	+5.44216
4	+0.38569	-2.31593
5	-0.12403	+1.25550
6	+1.53168	-0.27368

(b) $V_0 = +365.41359$

Note that for the torsion about C...O, only cosine functions are needed because the torsional potential is symmetric. However, the torsion about N...O leads to an asymmetric potential, and odd functions (sine functions) are required to obtain a good fit.

Thermal rate coefficients and branching ratios

Table S5: Variational, Γ^{CVT}, tunneling effects, $\kappa^{\mathrm{CVT/SCT}}_{E_0(\mathrm{R})}$ (in the LPL) and $\kappa^{\mathrm{CVT/SCT}}_{E_0(\mathrm{C1})}$ (in the HPL), harmonic-oscillator, $k^{\mathrm{TST,HO}}$, and anharmonic, $k^{\mathrm{TST,Anh}}$, TST rate constans, and CVT/SCT rate coefficients in the low-pressure, $k^{\mathrm{CVT/SCT}}_{\mathrm{LPL}}$, and high-pressure, $k^{\mathrm{CVT/SCT}}_{\mathrm{HPL}}$, regimes, for the hydrogen abstraction from the methyl group. Rate coefficients in $\mathrm{cm^3 molecule^{-1} s^{-1}}$.

T(K)	Γ^{CVT}	$\kappa^{\mathrm{CVT/SCT}}_{E_0(\mathrm{R})}$	$\kappa^{\mathrm{CVT/SCT}}_{E_0(\mathrm{C1})}$	$k^{\mathrm{TST,HO}}$	$k^{\mathrm{TST,Anh}}$	$k^{\mathrm{CVT/SCT}}_{\mathrm{LPL}}$	$k^{\mathrm{CVT/SCT}}_{\mathrm{HPL}}$
10	2.033e-20*	3.125e+22	8.143e+157	9.734e-15	5.337e-08	3.391e-05	8.836e+130
20	1.698e-10	6.659e+10	7.150e+72	2.346e-13	5.493e-10	6.211e-09	6.669e+53
30	3.864e-07	8.804e+06	2.925e+44	5.286e-13	9.324e-11	3.172e-10	1.054e+28
40	1.945e-05	1.033e+05	1.896e+30	7.148e-13	3.466e-11	6.964e-11	1.278e+15
50	2.093e-04	7.285e+03	6.045e+21	8.140e-13	1.826e-11	2.784e-11	2.310e+07
52	3.077e-04	4.760e+03	2.597e+20	8.276e-13	1.641e-11	2.403e-11	1.311e+06
60	1.033e-03	1.260e+03	1.379e+16	8.638e-13	1.166e-11	1.517e-11	1.660e+02
70	3.251e-03	3.635e+02	1.385e+12	8.876e-13	8.386e-12	9.910e-12	3.776e-02
76	5.605e-03	2.026e+02	1.871e+10	8.952e-13	7.168e-12	8.139e-12	7.517e-04
80	7.705e-03	1.444e+02	1.577e+09	8.984e-13	6.540e-12	7.276e-12	7.947e-05
89	1.430e-02	7.511e+01	1.529e+07	9.028e-13	5.484e-12	5.890e-12	1.199e-06
90	1.510e-02	7.095e+01	1.034e+07	9.032e-13	5.401e-12	5.787e-12	8.433e-07
100	2.588e-02	4.045e+01	2.731e+05	9.054e-13	4.653e-12	4.871e-12	3.288e-08
106	3.406e-02	3.047e+01	5.150e+04	9.066e-13	4.324e-12	4.487e-12	7.584e-09
107	3.555e-02	2.916e+01	4.050e+04	9.068e-13	4.275e-12	4.432e-12	6.155e-09
110	4.023e-02	2.570e+01	2.063e+04	9.074e-13	4.140e-12	4.280e-12	3.436e-09
120	5.811e-02	1.769e+01	3.295e+03	9.100e-13	3.777e-12	3.883e-12	7.232e-10
130	7.930e-02	1.296e+01	8.425e+02	9.138e-13	3.516e-12	3.613e-12	2.349e-10
135	9.104e-02	1.130e+01	4.841e+02	9.162e-13	3.413e-12	3.511e-12	1.504e-10
140	1.035e-01	9.965e+00	2.976e+02	9.192e-13	3.326e-12	3.430e-12	1.024e-10
150	1.303e-01	7.963e+00	1.322e+02	9.262e-13	3.189e-12	3.308e-12	5.492e-11
160	1.594e-01	6.565e+00	6.947e+01	9.352e-13	3.092e-12	3.235e-12	3.424e-11
170	1.903e-01	5.553e+00	4.133e+01	9.458e-13	3.025e-12	3.197e-12	2.379e-11
177	2.145e-01	4.967e+00	2.981e+01	9.548e-13	2.992e-12	3.187e-12	1.913e-11
180	2.227e-01	4.797e+00	2.701e+01	9.580e-13	2.983e-12	3.187e-12	1.794e-11
190	2.563e-01	4.218e+00	1.897e+01	9.720e-13	2.962e-12	3.202e-12	1.440e-11
200	2.907e-01	3.765e+00	1.409e+01	9.874e-13	2.956e-12	3.236e-12	1.211e-11
250	4.678e-01	2.499e+00	5.376e+00	1.088e-12	3.115e-12	3.642e-12	7.834e-12
300	6.390e-01	1.950e+00	3.221e+00	1.223e-12	3.482e-12	4.339e-12	7.166e-12
350	7.945e-01	1.660e+00	2.368e+00	1.390e-12	3.999e-12	5.274e-12	7.523e-12
400	9.313e-01	1.487e+00	1.939e+00	1.590e-12	4.643e-12	6.429e-12	8.384e-12
500	9.546e-01	1.299e+00	1.531e+00	2.090e-12	6.291e-12	7.802e-12	9.195e-12
600	9.296e-01	1.203e+00	1.345e+00	2.730e-12	8.408e-12	9.403e-12	1.051e-11
700	9.066e-01	1.147e+00	1.244e+00	3.528e-12	1.102e-11	1.146e-11	1.243e-11
800	8.879e-01	1.111e+00	1.182e+00	4.500e-12	1.417e-11	1.398e-11	1.487e-11
1000	8.608e-01	1.071e+00	1.113e+00	7.016e-12	2.210e-11	2.038e-11	2.118e-11

* 2.033e-20 means 2.033×10^{-20}

Table S6: Same as Table S5 but for the hydrogen abstraction from the amine group, being TS2a the transition state.

T(K)	Γ^{CVT}	$\kappa^{\mathrm{CVT/SCT}}_{E_0(\mathrm{R})}$	$\kappa^{\mathrm{CVT/SCT}}_{E_0(\mathrm{C2})}$	$k^{\mathrm{TST,HO}}$	$k^{\mathrm{TST,Anh}}$	$k^{\mathrm{CVT/SCT}}_{\mathrm{LPL}}$	$k^{\mathrm{CVT/SCT}}_{\mathrm{HPL}}$
10	3.337e-05	1.000e+00	1.024e+10	8.362e+07	6.295e+07	2.101e+03	2.151e+13
20	5.814e-03	1.000e+00	8.276e+04	2.042e-02	1.823e-02	1.060e-04	8.772e+00
30	3.276e-02	1.000e+00	1.424e+03	9.918e-06	9.820e-06	3.217e-07	4.581e-04
40	7.872e-02	1.000e+00	1.778e+02	1.963e-07	2.097e-07	1.651e-08	2.935e-06
50	1.346e-01	1.000e+00	5.037e+01	1.773e-08	1.998e-08	2.689e-09	1.354e-07
52	1.469e-01	1.000e+00	4.108e+01	1.198e-08	1.363e-08	2.002e-09	8.225e-08
60	1.938e-01	1.000e+00	2.171e+01	3.482e-09	4.071e-09	7.887e-10	1.712e-08
70	2.525e-01	1.000e+00	1.195e+01	1.075e-09	1.288e-09	3.253e-10	3.887e-09
76	2.868e-01	1.000e+00	9.032e+00	6.142e-10	7.436e-10	2.133e-10	1.926e-09
80	3.089e-01	1.000e+00	7.683e+00	4.428e-10	5.392e-10	1.666e-10	1.280e-09
89	3.574e-01	1.000e+00	5.635e+00	2.346e-10	2.884e-10	1.031e-10	5.808e-10
90	3.621e-01	1.000e+00	5.485e+00	2.218e-10	2.729e-10	9.879e-11	5.419e-10
100	4.115e-01	1.000e+00	4.217e+00	1.276e-10	1.579e-10	6.499e-11	2.740e-10
106	4.393e-01	1.000e+00	3.700e+00	9.634e-11	1.195e-10	5.250e-11	1.942e-10
107	4.438e-01	1.000e+00	3.626e+00	9.222e-11	1.144e-10	5.078e-11	1.841e-10
110	4.572e-01	1.000e+00	3.422e+00	8.130e-11	1.009e-10	4.615e-11	1.579e-10
120	4.992e-01	1.000e+00	2.891e+00	5.596e-11	6.955e-11	3.472e-11	1.004e-10
130	5.378e-01	1.000e+00	2.518e+00	4.092e-11	5.083e-11	2.734e-11	6.883e-11
135	5.559e-01	1.000e+00	2.373e+00	3.564e-11	4.423e-11	2.459e-11	5.835e-11
140	5.731e-01	1.000e+00	2.247e+00	3.138e-11	3.891e-11	2.230e-11	5.011e-11
150	6.052e-01	1.000e+00	2.044e+00	2.502e-11	3.094e-11	1.872e-11	3.827e-11
160	6.343e-01	1.000e+00	1.887e+00	2.058e-11	2.537e-11	1.609e-11	3.036e-11
170	6.609e-01	1.000e+00	1.763e+00	1.738e-11	2.135e-11	1.411e-11	2.487e-11
177	6.791e-01	1.000e+00	1.686e+00	1.554e-11	1.902e-11	1.292e-11	2.178e-11
180	6.850e-01	1.000e+00	1.663e+00	1.501e-11	1.835e-11	1.257e-11	2.091e-11
190	7.070e-01	1.000e+00	1.583e+00	1.320e-11	1.608e-11	1.136e-11	1.799e-11
200	7.269e-01	1.000e+00	1.516e+00	1.179e-11	1.430e-11	1.039e-11	1.576e-11
250	8.029e-01	1.000e+00	1.307e+00	7.982e-12	9.466e-12	7.600e-12	9.933e-12
300	8.475e-01	1.000e+00	1.164e+00	6.484e-12	7.528e-12	6.380e-12	7.427e-12
350	8.701e-01	1.000e+00	1.119e+00	5.838e-12	6.649e-12	5.785e-12	6.474e-12
400	8.849e-01	1.000e+00	1.091e+00	5.594e-12	6.261e-12	5.540e-12	6.045e-12
500	8.926e-01	1.000e+00	1.058e+00	5.702e-12	6.192e-12	5.526e-12	5.847e-12
600	8.878e-01	1.000e+00	1.040e+00	6.246e-12	6.606e-12	5.864e-12	6.099e-12
700	8.824e-01	1.000e+00	1.029e+00	7.074e-12	7.304e-12	6.445e-12	6.631e-12
800	8.708e-01	1.000e+00	1.022e+00	8.132e-12	8.209e-12	7.149e-12	7.306e-12
1000	8.597e-01	1.000e+00	1.014e+00	1.088e-11	1.053e-11	9.055e-12	9.182e-12

Table S7: Same as Table S6 but for TS2b.

T(K)	Γ^{CVT}	$\kappa^{\mathrm{CVT/SCT}}_{E_0(\mathrm{R})}$	$\kappa^{\mathrm{CVT/SCT}}_{E_0(\mathrm{C2})}$	$k^{\mathrm{TST,HO}}$	$k^{\mathrm{TST,Anh}}$	$k^{\mathrm{CVT/SCT}}_{\mathrm{LPL}}$	$k^{\mathrm{CVT/SCT}}_{\mathrm{HPL}}$
10	4.856e-06	1.000e+00	1.339e+12	3.440e+06	7.235e+07	3.514e+02	4.705e+14
20	2.216e-03	1.000e+00	8.345e+05	4.154e-03	1.962e-02	4.347e-05	3.628e+01
30	1.709e-02	1.000e+00	6.120e+03	3.410e-06	1.033e-05	1.765e-07	1.080e-03
40	4.774e-02	1.000e+00	5.009e+02	8.670e-08	2.181e-07	1.041e-08	5.215e-06
50	8.882e-02	1.000e+00	1.108e+02	8.998e-09	2.064e-08	1.834e-09	2.032e-07
52	9.823e-02	1.000e+00	8.697e+01	6.210e-09	1.406e-08	1.381e-09	1.201e-07
60	1.348e-01	1.000e+00	4.084e+01	1.922e-09	4.185e-09	5.641e-10	2.304e-08
70	1.820e-01	1.000e+00	2.025e+01	6.268e-10	1.321e-09	2.403e-10	4.866e-09
76	2.099e-01	1.000e+00	1.461e+01	3.668e-10	7.616e-10	1.599e-10	2.336e-09
80	2.282e-01	1.000e+00	1.210e+01	2.680e-10	5.518e-10	1.259e-10	1.523e-09
89	2.681e-01	1.000e+00	8.460e+00	1.454e-10	2.947e-10	7.900e-11	6.683e-10
90	2.720e-01	1.000e+00	8.201e+00	1.378e-10	2.788e-10	7.582e-11	6.218e-10
100	3.126e-01	1.000e+00	6.062e+00	8.084e-11	1.612e-10	5.041e-11	3.056e-10
106	3.349e-01	1.000e+00	5.218e+00	6.160e-11	1.219e-10	4.084e-11	2.131e-10
107	3.386e-01	1.000e+00	5.098e+00	5.906e-11	1.168e-10	3.953e-11	2.015e-10
110	3.487e-01	1.000e+00	4.771e+00	5.226e-11	1.030e-10	3.591e-11	1.713e-10
120	3.812e-01	1.000e+00	3.933e+00	3.640e-11	7.093e-11	2.704e-11	1.063e-10
130	4.145e-01	1.000e+00	3.357e+00	2.686e-11	5.182e-11	2.148e-11	7.211e-11
135	4.302e-01	1.000e+00	3.135e+00	2.348e-11	4.509e-11	1.940e-11	6.081e-11
140	4.454e-01	1.000e+00	2.944e+00	2.074e-11	3.964e-11	1.766e-11	5.198e-11
150	4.743e-01	1.000e+00	2.637e+00	1.663e-11	3.152e-11	1.495e-11	3.942e-11
160	5.012e-01	1.000e+00	2.402e+00	1.375e-11	2.584e-11	1.295e-11	3.111e-11
170	5.261e-01	1.000e+00	2.218e+00	1.166e-11	2.174e-11	1.144e-11	2.537e-11
177	5.438e-01	1.000e+00	2.104e+00	1.045e-11	1.937e-11	1.054e-11	2.217e-11
180	5.496e-01	1.000e+00	2.070e+00	1.010e-11	1.869e-11	1.027e-11	2.126e-11
190	5.711e-01	1.000e+00	1.950e+00	8.908e-12	1.637e-11	9.348e-12	1.823e-11
200	5.915e-01	1.000e+00	1.851e+00	7.978e-12	1.456e-11	8.610e-12	1.594e-11
250	6.713e-01	1.000e+00	1.327e+00	5.442e-12	9.627e-12	6.463e-12	8.576e-12
300	7.130e-01	1.000e+00	1.222e+00	4.436e-12	7.647e-12	5.452e-12	6.663e-12
350	7.428e-01	1.000e+00	1.160e+00	4.000e-12	6.745e-12	5.010e-12	5.812e-12
400	7.688e-01	1.000e+00	1.122e+00	3.834e-12	6.342e-12	4.876e-12	5.471e-12
500	7.884e-01	1.000e+00	1.077e+00	3.904e-12	6.251e-12	4.929e-12	5.308e-12
600	7.882e-01	1.000e+00	1.053e+00	4.272e-12	6.655e-12	5.245e-12	5.523e-12
700	7.879e-01	1.000e+00	1.039e+00	4.834e-12	7.346e-12	5.788e-12	6.013e-12
800	7.731e-01	1.000e+00	1.030e+00	5.554e-12	8.248e-12	6.376e-12	6.568e-12
1000	7.692e-01	1.000e+00	1.019e+00	7.428e-12	1.057e-11	8.132e-12	8.286e-12

Table S8: Rate coefficients (in $cm^3molecule^{-1}s^{-1}$) of association, k_a, CVT/SCT, $k_{H,j}^{CVT/SCT}$, and CCUS, k_j^{CCUS}, for R1 ($j = 1$) and R2 ($j = 2$) in the low-pressure limit. The global rate coefficient k^{CCUS} is also given.

T(K)	k_a	$k_{H,1}^{CVT/SCT}$	k_1^{CCUS}	$k_{H,2}^{CVT/SCT}$	k_2^{CCUS}	k^{CCUS}
10	6.192e-10	3.391e-05	8.564e-18	2.452e+03	6.192e-10	6.192e-10
20	5.517e-10	6.211e-09	2.293e-14	1.495e-04	5.517e-10	5.517e-10
30	5.156e-10	3.172e-10	3.277e-13	4.983e-07	5.148e-10	5.151e-10
40	4.915e-10	6.964e-11	1.245e-12	2.692e-08	4.815e-10	4.827e-10
50	4.735e-10	2.784e-11	2.624e-12	4.522e-09	4.263e-10	4.289e-10
52	4.703e-10	2.403e-11	2.915e-12	3.383e-09	4.104e-10	4.133e-10
60	4.594e-10	1.517e-11	3.814e-12	1.353e-09	3.401e-10	3.439e-10
70	4.477e-10	9.910e-12	4.336e-12	5.656e-10	2.475e-10	2.518e-10
76	4.416e-10	8.139e-12	4.368e-12	3.731e-10	2.002e-10	2.046e-10
80	4.379e-10	7.276e-12	4.319e-12	2.925e-10	1.736e-10	1.779e-10
89	4.301e-10	5.890e-12	4.099e-12	1.821e-10	1.267e-10	1.308e-10
90	4.294e-10	5.787e-12	4.075e-12	1.746e-10	1.230e-10	1.270e-10
100	4.219e-10	4.871e-12	3.790e-12	1.154e-10	8.979e-11	9.358e-11
106	4.178e-10	4.487e-12	3.636e-12	9.333e-11	7.563e-11	7.926e-11
107	4.172e-10	4.432e-12	3.612e-12	9.032e-11	7.360e-11	7.721e-11
110	4.152e-10	4.280e-12	3.544e-12	8.205e-11	6.793e-11	7.147e-11
120	4.093e-10	3.883e-12	3.346e-12	6.176e-11	5.322e-11	5.657e-11
130	4.038e-10	3.613e-12	3.198e-12	4.882e-11	4.321e-11	4.640e-11
135	4.013e-10	3.511e-12	3.140e-12	4.399e-11	3.933e-11	4.247e-11
140	3.989e-10	3.430e-12	3.094e-12	3.996e-11	3.604e-11	3.913e-11
150	3.943e-10	3.308e-12	3.025e-12	3.367e-11	3.079e-11	3.381e-11
160	3.901e-10	3.235e-12	2.988e-12	2.904e-11	2.682e-11	2.981e-11
170	3.862e-10	3.197e-12	2.975e-12	2.554e-11	2.377e-11	2.675e-11
177	3.834e-10	3.187e-12	2.980e-12	2.346e-11	2.193e-11	2.491e-11
180	3.825e-10	3.187e-12	2.984e-12	2.284e-11	2.139e-11	2.437e-11
190	3.791e-10	3.202e-12	3.012e-12	2.071e-11	1.948e-11	2.250e-11
200	3.759e-10	3.236e-12	3.055e-12	1.901e-11	1.794e-11	2.100e-11
250	3.621e-10	3.642e-12	3.472e-12	1.406e-11	1.341e-11	1.688e-11
300	3.513e-10	4.339e-12	4.148e-12	1.183e-11	1.131e-11	1.546e-11
350	3.424e-10	5.274e-12	5.037e-12	1.080e-11	1.031e-11	1.535e-11
400	3.348e-10	6.429e-12	6.121e-12	1.042e-11	9.917e-12	1.604e-11
500	3.226e-10	7.802e-12	7.384e-12	1.045e-11	9.895e-12	1.728e-11
600	3.130e-10	9.403e-12	8.825e-12	1.111e-11	1.043e-11	1.925e-11
700	3.050e-10	1.146e-11	1.064e-11	1.223e-11	1.135e-11	2.199e-11
800	2.983e-10	1.398e-11	1.280e-11	1.353e-11	1.238e-11	2.518e-11
1000	2.874e-10	2.038e-11	1.802e-11	1.719e-11	1.520e-11	3.322e-11

Table S9: Same as Table S8 but for the high-pressure limit.

T(K)	k_{a}	$k_{\mathrm{H},1}^{\mathrm{CVT/SCT}}$	k_1^{CCUS}	$k_{\mathrm{H},2}^{\mathrm{CVT/SCT}}$	k_2^{CCUS}	k^{CCUS}
10	6.192e-10	8.836e+130	6.192e-10	4.920e+14	3.448e-126	6.192e-10
20	5.517e-10	6.669e+53	5.517e-10	4.505e+01	3.726e-62	5.517e-10
30	5.156e-10	1.054e+28	5.156e-10	1.539e-03	7.528e-41	5.156e-10
40	4.915e-10	1.278e+15	4.915e-10	8.151e-06	3.134e-30	4.915e-10
50	4.735e-10	2.310e+07	4.735e-10	3.386e-07	6.941e-24	4.735e-10
52	4.703e-10	1.311e+06	4.703e-10	2.024e-07	7.259e-23	4.703e-10
60	4.594e-10	1.660e+02	4.594e-10	4.016e-08	1.111e-19	4.594e-10
70	4.477e-10	3.776e-02	4.477e-10	8.753e-09	1.038e-16	4.477e-10
76	4.416e-10	7.517e-04	4.416e-10	4.262e-09	2.504e-15	4.416e-10
80	4.379e-10	7.947e-05	4.378e-10	2.803e-09	1.545e-14	4.379e-10
89	4.301e-10	1.199e-06	4.295e-10	1.249e-09	4.474e-13	4.299e-10
90	4.294e-10	8.433e-07	4.285e-10	1.164e-09	5.913e-13	4.291e-10
100	4.219e-10	3.288e-08	4.094e-10	5.796e-10	7.216e-12	4.166e-10
106	4.178e-10	7.584e-09	3.768e-10	4.073e-10	2.024e-11	3.970e-10
107	4.172e-10	6.155e-09	3.690e-10	3.857e-10	2.312e-11	3.921e-10
110	4.152e-10	3.436e-09	3.413e-10	3.292e-10	3.270e-11	3.740e-10
120	4.093e-10	7.232e-10	2.210e-10	2.067e-10	6.317e-11	2.842e-10
130	4.038e-10	2.349e-10	1.217e-10	1.409e-10	7.300e-11	1.947e-10
135	4.013e-10	1.504e-10	8.998e-11	1.192e-10	7.128e-11	1.613e-10
140	3.989e-10	1.024e-10	6.772e-11	1.021e-10	6.748e-11	1.352e-10
150	3.943e-10	5.492e-11	4.110e-11	7.769e-11	5.814e-11	9.924e-11
160	3.901e-10	3.424e-11	2.749e-11	6.147e-11	4.936e-11	7.685e-11
170	3.862e-10	2.379e-11	1.997e-11	5.024e-11	4.216e-11	6.212e-11
177	3.834e-10	1.913e-11	1.643e-11	4.395e-11	3.774e-11	5.417e-11
180	3.825e-10	1.794e-11	1.551e-11	4.217e-11	3.644e-11	5.195e-11
190	3.791e-10	1.440e-11	1.270e-11	3.622e-11	3.195e-11	4.466e-11
200	3.759e-10	1.211e-11	1.085e-11	3.170e-11	2.839e-11	3.923e-11
250	3.621e-10	7.834e-12	7.303e-12	1.851e-11	1.725e-11	2.456e-11
300	3.513e-10	7.166e-12	6.757e-12	1.409e-11	1.329e-11	2.004e-11
350	3.424e-10	7.523e-12	7.111e-12	1.229e-11	1.161e-11	1.872e-11
400	3.348e-10	8.384e-12	7.913e-12	1.152e-11	1.087e-11	1.878e-11
500	3.226e-10	9.195e-12	8.649e-12	1.116e-11	1.049e-11	1.914e-11
600	3.130e-10	1.051e-11	9.818e-12	1.162e-11	1.085e-11	2.067e-11
700	3.050e-10	1.243e-11	1.149e-11	1.264e-11	1.168e-11	2.317e-11
800	2.983e-10	1.487e-11	1.356e-11	1.387e-11	1.265e-11	2.622e-11
1000	2.874e-10	2.118e-11	1.867e-11	1.747e-11	1.540e-11	3.407e-11

Table S10: Branching ratios in the low-pressure (LP) and high-pressure (HP) limits.

T(K)	$\left(\frac{k_1^{CCUS}}{k^{CCUS}}\right)_{LPL}$	$\left(\frac{k_2^{CCUS}}{k^{CCUS}}\right)_{LPL}$	$\left(\frac{k_1^{CCUS}}{k^{CCUS}}\right)_{HPL}$	$\left(\frac{k_2^{CCUS}}{k^{CCUS}}\right)_{HPL}$
10	0	100	100	0
20	0	100	100	0
30	0	100	100	0
40	0	100	100	0
50	1	99	100	0
52	1	99	100	0
60	1	99	100	0
70	2	98	100	0
76	2	98	100	0
80	2	98	100	0
89	3	97	100	0
90	3	97	100	0
100	4	96	98	2
106	5	95	95	5
107	5	95	94	6
110	5	95	91	9
120	6	94	78	22
130	7	93	62	38
135	7	93	56	44
140	8	92	50	50
150	9	91	41	59
160	10	90	36	64
170	11	89	32	68
177	12	88	30	70
180	12	88	30	70
190	13	87	28	72
200	15	85	28	72
250	21	79	30	70
300	27	73	34	66
350	33	67	38	62
400	38	62	42	58
500	43	57	45	55
600	46	54	47	53
700	48	52	50	50
800	51	49	52	48
1000	54	46	55	45